Chinese Chemical Letters 32 (2021) 1106–1110

Contents lists available at ScienceDirect

Chinese Chemical Letters

journal homepage: www.elsevier.com/locate/cclet

Communication

Porous carbon framework nested nickel foam as freestanding host for high energy lithium sulfur batteries

Yan Song[a,b], Xiuyuan Li[a,b], Chaozheng He[a,b,*]

[a] Shaanxi Key Laboratory of Optoelectronic Functional Materials and Devices, School of Materials Science and Chemical Engineering, Xi'an Technological University, Xi'an 710021, China
[b] Institute of Environmental and Energy Catalysis, School of Materials Science and Chemical Engineering, Xi'an Technological University, Xi'an 710021, China

ARTICLE INFO

Article history:
Received 21 July 2020
Received in revised form 26 July 2020
Accepted 17 August 2020
Available online 19 August 2020

Keywords:
Porous carbon
Nitrogen doping
Polysulfides anchoring
Freestanding electrode
Lithium–sulfur batteries

ABSTRACT

Constructing 3D multifunctional conductive framework as stable sulfur cathode contributes to develop advanced lithium-sulfur (Li-S) batteries. Herein, a freestanding electrode with nickel foam framework and nitrogen doped porous carbon (PC) network is presented to encapsulate active sulfur for Li-S batteries. In such a mutually embedded architecture with high stability, the interconnected carbon network and nickel foam matrix can expedite ionic/electronic transport and sustain volume variations of sulfur. Furthermore, rationally designed porous structures provide sufficient internal space and large surface area for high active sulfur loading and polar polysulfides anchoring. Benefiting from the synergistic superiority, the Ni/PC-S cathode exhibits a high initial capacity of around 1200 mAh/g at 0.2 C, excellent rate performance, and high cycling stability with a low decay rate of 0.059% per cycle after 500 cycles. This work provides a useful strategy to exploit freestanding porous framework for diverse applications.

Lithium–sulfur battery as a high energy density storage device has been considered as a promising next-generation rechargeable system by virtue of high theoretical specific capacity (1675 mAh/g) and energy density (2567 Wh/kg) [1–3]. Although the high energy density is attractive, the commercial realization of rechargeable Li-S battery is still impeded by dissolution and shuttle of soluble lithium polysulfide (Li_2S_x, $4 \leq x \leq 8$), poor electronic conductivity of active materials, sluggish redox kinetics, and volume expansion of cathode during discharge [4–6]. Thereinto, the shuttle effect of polysulfide not only results in devolution of active materials for sulfur cathode but also poisons the lithium metal anode, which eventually induces fast capacity degradation and low Coulombic efficiency [7,8].

To resolve abovementioned issues, numerous efforts have been devoted to design and construct micro-nanostructure architectures for encapsulation of active sulfur [9,10]. For ideal architectures loaded by sulfur, essential characteristics should be equipped, including high electrical conductivity to reduce the polarization resistance of electrode, large specific surface area to provide plentiful anchor sites for polysulfides, abundant porous structure to realize high sulfur loading and buffer the volumetric variations of sulfur [11–14]. Because of the excellent electron conductivity and stability, carbon-based encapsulation materials can greatly improve the electronic conductivity of electrodes and avoid the volume expansion of active materials, which demonstrates high active material utilization and remarkable cycle stability [15,16]. Porous carbon materials as one of the most promising hosts possess above advantages and have achieve remarkable results on improvements of battery capacity and cyclability [17–20]. Heteroatom dopings such as B, N, O, P and S atoms can effectively improve the polarity and sulfiphilic affinity of porous carbon, which are beneficial to prevent the migration of soluble polysulfides and reduce the need for infiltrated electrolyte [21–26].

Nevertheless, for traditional sulfur cathodes, the inclusions of binder, conductive additives, and metal current collector increase the manufacturing cost and restricts the actual energy density. In recent years, based on the inherent structural advantage, the materials with two-dimensional (2D) and three-dimensional (3D) structure are widely studied to facilitate the transportation of electrons and ions and improve the electrochemical performance of energy storage systems [27–29]. Furthermore, 3D frameworks with high electronic conductivity are considered as self-supporting hosts for high sulfur loading [30–33]. Compared with the

* Corresponding author at: Shaanxi Key Laboratory of Optoelectronic Functional Materials and Devices, School of Materials Science and Chemical Engineering, Xi'an Technological University, Xi'an 710021, China.
E-mail address: hecz2019@xatu.edu.cn (C. He).

https://doi.org/10.1016/j.cclet.2020.08.024
1001-8417/

traditional electrodes, the 3D foam electrode with relatively large surface area can provide electric contact sites to promote redox reaction kinetics and uniform deposition of active materials [34]. Furthermore, 3D conductive matrix can shorten the migration path of electrons and lithium ions to reduce polarization resistance [35–37]. Therefore, the design of self-supporting cathodes with 3D framework is highly desirable for realizing high energy density Li–S batteries.

Herein, we propose a feasible and scalable approach for constructing a freestanding electrode with nickel foam framework and nitrogen doped porous carbon (PC) network. Nickel foam as a freestanding interconnected matrix provides efficient channels for electron transport and increases the cathode conductivity. The porous architecture of PC provides sufficient internal space and large surface area for high active sulfur loading and electrolytic infiltration. Simultaneously, 3D carbon architecture with a unique interconnected microstructure is beneficial to retention of polysulfide by physical confinement. Furthermore, the carbon network is doped by nitrogen heteroatoms, which expedites electron transport for improving kinetics of the electrochemical reactions and facilitates anchoring effect for polar polysulfides based on chemical interactions. The synergistic morphology and structure engineering of nickel foam framework and PC network boosts the sulfur utilization and cycling stability. This study heralds a new avenue to exploit freestanding porous electrode for high-volume energy storage systems.

Fig. 1a presents the schematic diagram of fabrication procedure for Ni/PC-S freestanding electrode with interconnected network architecture. First, porous Ni/PAN was synthesized by nesting PAN collosol with urea onto nickel foam and boiling process. In the collosol, PAN and urea serve as carbon source and space-holder, respectively. After followed carbonization strategy, the Ni/PC hierarchical porous framework was obtained based on the *in situ* chemical conversion process. Finally, active sulfur was loaded into the Ni/PC porous framework *via* the solution and melt diffusion methods. The morphology of Ni/PAN and Ni/PC were characterized by scanning electron microscopy (SEM). As revealed in Figs. 1b-d, the PAN filled into nickel foam to form Ni/PAN with continuous 3D backbone and interconnected PAN porous network. The rationally designed Ni/PC inherits similar structure and morphology as Ni/PAN, manifesting the carbonization do not destroy the porous architecture. The difference between Ni/PAN and Ni/PC is that the crevice is observed on the surface of Ni/PC (Fig. 1e), which is beneficial to electrolytic infiltration. Moreover, the interconnected porous carbon network of Ni/PC (Figs. 1f and g) could not only provides fast electron and ion transport pathways, but also relieves volume swelling during lithiation.

After filling with sulfur, the interconnected network structure is still maintained, and sulfur particles are loaded on the surface of carbon framework, as presented in Figs. 2a and b. From elemental mapping results in Fig. 2c, the distribution of sulfur is rather homogeneous within the carbon network architecture. Furthermore, the nitrogen element is also uniformly distributed on the carbon framework, which can promote electrode conductivity. Homogeneous dispersion of polar nitrogen atom and large surface area of carbon endow cathode with abundant anchoring sites for confining polysulfides.

X-ray diffraction (XRD) pattern of as-prepared Ni/PC sample (Fig. 2d) demonstrates the sharp peaks at 44.3° and 51.7° corresponding to (111) and (200) phases of Ni and a broad characteristic peak at about 26° corresponding to PC with amorphous nature. After incorporated sulfur into the Ni/PC framework, the diffraction peaks with weak intensity between 20° to 30° can be assigned to orthorhombic sulfur (JCPDS No. 85–0799), which suggest that the sulfur is uniformly deposited into the porous structure. The specific sulfur content is confirmed the thermogravimetric analysis (TGA). As revealed in the TGA curve of Ni/PC-S (Fig. S1 in Supporting information), the amount of sulfur incorporated into Ni/PC framework is close to the theoretical 75% loading determined from the cathode preparation protocol.

X-ray photoelectron spectroscopy (XPS) was carried out to ascertain the surface chemical composition of Ni/PC—S and the chemical adsorption sites of carbon framework. The refined C 1s XPS spectrum (Fig. 3a) can be deconvolved into three peaks at 284.6, 285.9 and 286.9 eV, which are attributed to the C—C/C=C, C—S and C—N bonds, respectively. The presence of C—S bond signifies the chemical interaction and fast charge transfer between sulfur and carbon framework. As shown in Fig. 3b, the high-resolution N 1s spectrum is composed of three different types of nitrogen defects centered at 398.1, 400.4 and 402.3 eV, which are attributed to pyridinic N, pyrrolic N, and graphitic N, respectively [12]. The ratios of pyridinic N, pyrrolic N and graphitic N are estimated to be 47.7%, 43.9% and 8.4% according to the XPS peak area analysis, respectively. These polar N are conducive to improve the affinity of carbon framework and contribute abundant anchoring sites for capturing the polar polysulfides by the electron delocalization effect. For the high-resolution S 2p XPS spectrum, the signals centered at 163.5, 164.7 and 168.6 eV corresponds to S $2p_{1/2}$, S $2p_{3/2}$ and sulfate, respectively [38]. The peaks of S $2p_{1/2}$ and S $2p_{3/2}$ shift to lower binding energy in comparison to the corresponding peaks of elemental sulfur (centered at 163.9 eV and 165.1 eV), indicating that the electron transfers from sulfur to carbon host [39].

Nitrogen adsorption/desorption experiments were conducted to define the specific surface area of Ni/PC framework (Fig. 3d). The

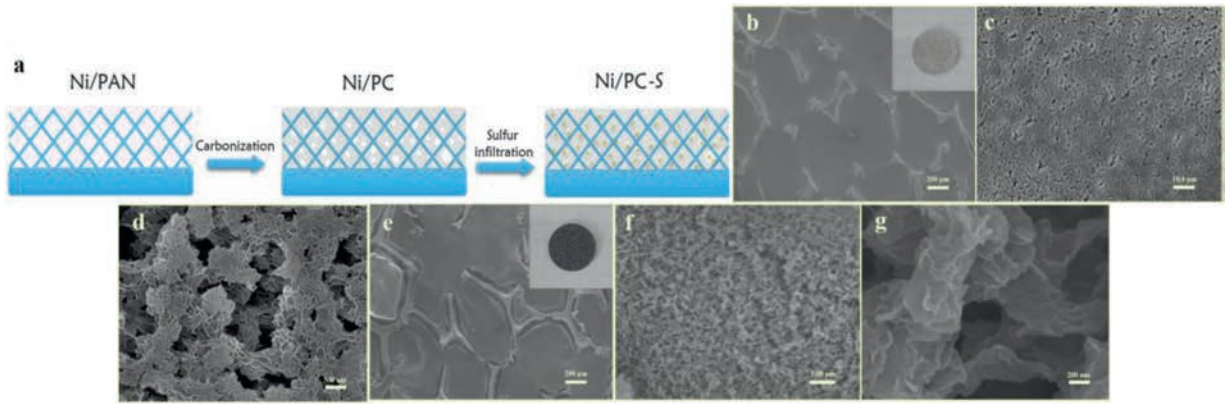

Fig. 1. (a) Schematic diagram for synthesis procedure of synthesis procedure. SEM images of (b-d) Ni/PAN and (e-g) Ni/PC.

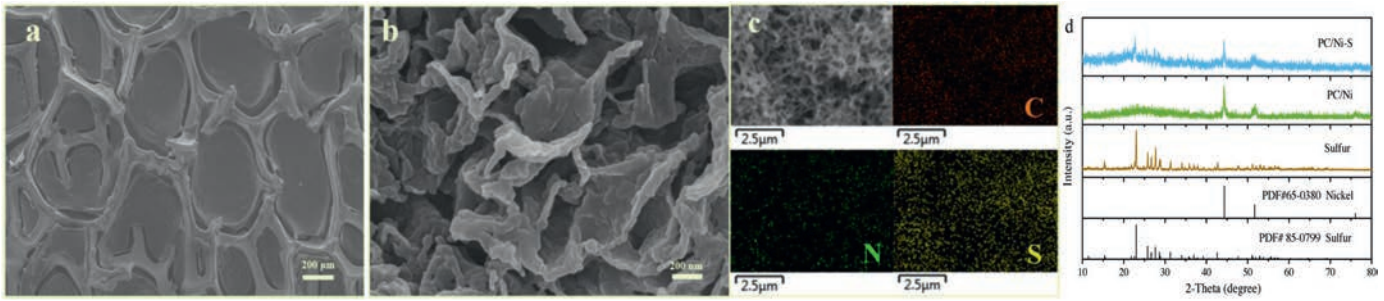

Fig. 2. (a, b) SEM images of Ni/PC-S electrode. (c) EDX elemental mapping of carbon, nitrogen, and sulfur in the Ni/PC-S. (d) XRD patterns of pure sulfur, Ni/PC and Ni/PC-S.

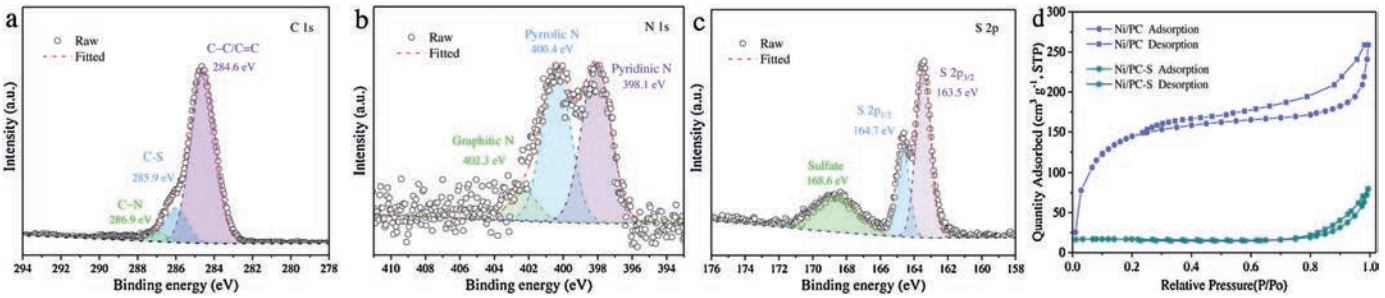

Fig. 3. High-resolution XPS spectra at (a) C 1s, (b) N 1s and (c) S 2p of Ni/PC-S. (d) Nitrogen adsorption/desorption isotherms of Ni/PC and Ni/PC-S.

Ni/PC exhibits a type IV isotherm with a sharp uptake in the low relative pressure region ($P/P_0 < 0.05$) and distinctive hysteresis within the relative pressure range ($0.3 < P/P_0 < 1.0$), revealing the existence of porous microstructure, which can promote the ion transport. According to the Brunauer-Emmett-Teller (BET) theory, the specific surface area of Ni/PC is deduced to be 813.5 m^2/g. High BET surface area is conducive to deposit uniform active sulfur and contribute sufficient anchoring sites for immobilizing polysulfides. After the impregnation of sulfur particles, the surface area decreases to 120.7 m^2/g, indicating that sulfur was smoothly immersed into the internal cavities of Ni/PC framework.

To systematically evaluate the electrochemical performance of Ni/PC-S cathodes, the 2032-type coin cells were assembled. For comparison, a sulfur cathode was fabricated by directly loading the sulfur slurry onto the nickel foam under the same conditions. As shown in Fig. 4a, the cyclic voltammetry (CV) curves of Ni/PC-S cathode exhibit that two cathodic peaks (I and II) located around 2.34 V and 2.04 V are assigned to the reduction of sulfur to soluble

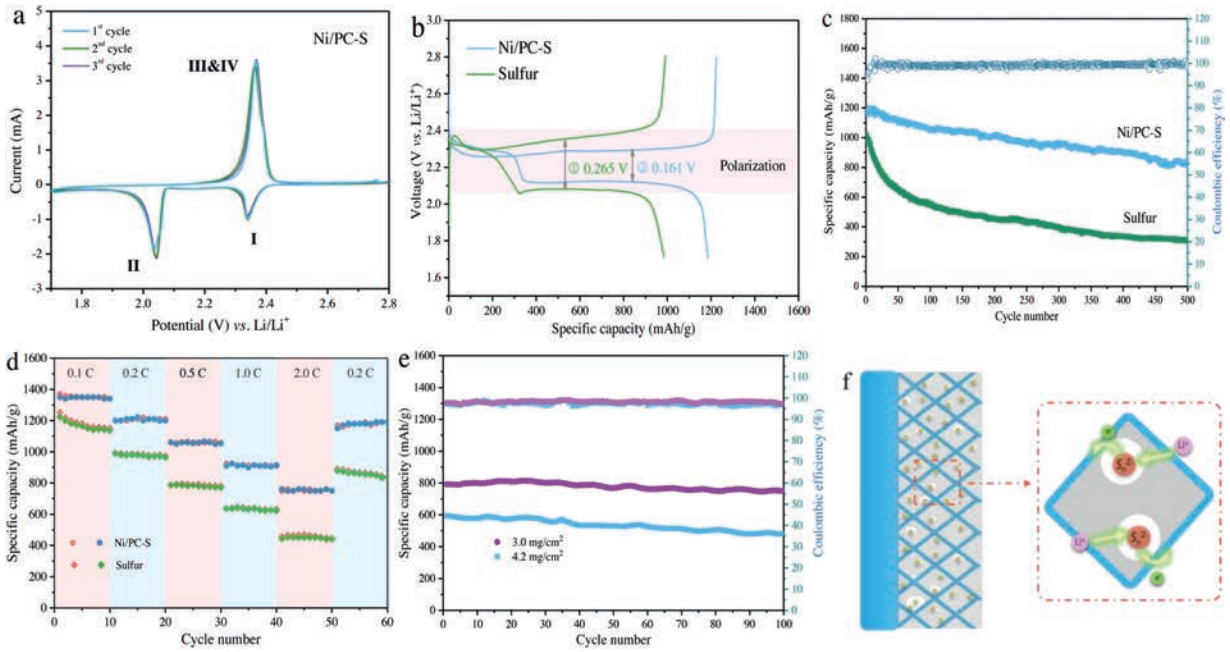

Fig. 4. (a) Typical CV profiles of Ni/PC-S electrode at 0.1 mV/s. (b) Galvanostatic charge–discharge curves of the first cycle for sulfur and Ni/PC-S cathodes at 0.2 C. (c) Cycling performances of sulfur and Ni/PC-S cathodes at 0.2 C for 500 cycles. (d) Rate capabilities at different rates of sulfur and Ni/PC-S cathodes. (e) Cycling performance of the Ni/PC-S cathodes with different high sulfur loadings at 1 C. (f) Schematic illustration of the structure for the Ni/PC-S electrode and the multipath rapid electron transfer for highly efficient redox reaction.

Li_2S_x and the further transformation from Li_2S_x to short-chain lithium sulfides (Li_2S_2 or Li_2S), and one anodic peak (III&IV) at around 2.37 V is related to the oxidation of lithium sulfides to sulfur. However, the CV curves of sulfur cathode (Fig. S2 in Supporting information) reveal widened redox peaks and larger peak separation between the cathodic and anodic peaks. Clearly, Ni/PC as host facilitates upshifts of voltage potential at cathodic peak and the downshifts at anodic peak, which suggests the smaller electrochemical polarization and rapid conversion kinetics [40]. As an important influence factor on the conversion kinetics, lithium ion diffusion coefficients are determined by CV tests at various scanning rates from 0.1 mV/s to 0.4 mV/s (Fig. S3 in Supporting information). All anodic and cathodic peaks currents are linear relationship with square root of scan rates, and the slope reflects the lithium ion diffusivity that can be estimated by the classical Randles–Sevcik equation [22]: $I_p = 2.69 \times 10^5 n^{1.5} S D_{Li}^{0.5} C_{Li} \nu^{0.5}$, where I_p is the peak current, n is the numbers of transfer electrons, S is the active electrode area, D_{Li} is the lithium ions diffusion coefficient, C_{Li} is the concentration of lithium ions, and ν is the scan rate. The calculated D_{Li} for anodic and cathodic peaks are 4.15×10^{-8}, 1.65×10^{-8} and 1.34×10^{-8} cm^2/s. The high lithium ions diffusion coefficients demonstrate that Ni/PC-S electrode has excellent reaction kinetics by virtue of effective adsorption sites and conductive framework.

Galvanostatic discharge–charge curves at 0.2 C (1 C = 1675 mA/g) of sulfur and Ni/PC-S cathodes show two discharging plateaus and a long charging plateau (Fig. 4b), in agreement with the CV results according to the multistep redox reaction. Note that, the tested CV and galvanostatic discharge-charge curve of pure Ni/PC cathode have negligible reduction and oxidation peaks and charge-discharge capacity (Figs. S4 and S5 in Supporting information), suggesting that Ni/PC as electrode exerts little contribution to the capacity. The Ni/PC-S cathode delivers an initial discharge capacity of about 200 mAh/g higher compared with the sulfur cathode, indicating that Ni/PC framework can elevate sulfur utilization during cycling. More importantly, for Ni/PC-S cathode, a smaller voltage gap (0.161 V) between discharging and charging plateau is obtained compared with that of sulfur cathode (0.265 V). It is demonstrated that porous network architecture of Ni/PC expedites electron transport for decreasing polarization during charge-discharge cycles. From the magnified discharge curves (Fig. S6 in Supporting information), the Ni/PC-S cathode obviously alleviates the interfacial energy barrier of 25 mV, which elucidates that the nucleation and deposition of Li_2S reaction are improved on the interface of carbon framework [23,41]. Fig. 4c shows the cycling performances of the Ni/PC-S and sulfur cathode at 0.2 C. It is obviously observed that the sulfur cathode suffers from a fast capacity decay of 0.14% per cycle after 500 cycles. In comparison, the Ni/PC-S cathode exhibits excellent cycling stability with 70.5% capacity retention and slow capacity fading rate of 0.059% per cycle after 500 cycles. Simultaneously, Coulombic efficiency of above 99% further indicates that Ni/PC promotes the utilization of the active materials and reversibility of the electrode reaction.

The rate performances of Ni/PC-S and sulfur cathode were evaluated at different current rates from 0.1 C to 2 C (Fig. 4d and Fig. S7 in Supporting information). Higher utilization of the active sulfur endows Ni/PC-S electrode with a discharge capacity of 1350 mAh/g at 0.1 C, and reversible capacities of 760 mAh/g can be achieved at a high current rate of 2 C. When the rate is returned back to 0.2 C, a higher discharge specific capacity of around 1150 mAh/g can be still obtained, suggesting the stability and reversibility of the electrode. The corresponding discharge–charge curves of Ni/PC-S electrode still contain two typical discharge plateaus along with the increase of rate (Fig. S8 in Supporting information). However, the discharge plateaus are short and unconspicuous at high current rate of 2 C for sulfur electrode. The excellent rate capability indicates that the Ni/PC backbone can accelerates ion diffusion and immobilize polysulfide to enhance sulfuric utilization. The colour of PP separator after cycles is used to further confirm the adsorption capacity of Ni/PC for polysulfide (Fig. S9 in Supporting information). It is note that delicate colour is observed after the cycles of the cell with Ni/PC-S cathode, which indicates excellent capturing capacity of porous framework for polysulfides. The electrochemical impedance spectra (EIS) of the Ni/PC-S electrode before and after the cycles show smaller charge transfer resistance (R_{ct}) and interface resistance (R_i) than that of sulfur electrode (Fig. S10 in Supporting information), which manifest that the Ni/PC backbone contributes to decrease polarization and improve rate performance by promoting electrolyte infiltration and electron transference [42,43]. The severe self-discharge induced by shuttle effect of polysulfides was also investigated by detecting the variation of the open circuit voltages (OCV) during the 48 h rest time. The evolution of OCVs with time for the cells is shown in Fig. S11 (Supporting information). The OCV suffers a drastic decline to 2.10 V for sulfur cathode due to the spontaneous reduction of polysulfides. In contrast, the OCV of Ni/PC-S cathode reveals a slight decrease and stabilizes at 2.38 V, indicating that Ni/PC can effectively suppress polysulfides shuttling to alleviate the self-discharge behavior of Li-S batteries [44,45].

For satisfying the practical application, cycling stabilities of Ni/PC-S electrodes with the sulfur loading of 3.0 and 4.2 mg/cm^2 were also evaluated, as presented in Fig. 4e. With the sulfur loading of 3.0 mg/cm^2, Ni/PC-S electrode delivers a decent capacity of nearly 800 mAh/g at 1 C, as well as 750 mAh/g after 100 cycles. Upon increasing the sulfur loading to 4.2 mg/cm^2, an initial capacity of 600 mAh/g and capacity retentions of 84.2% after 100 cycles can be retained. All these results show that Ni/PC-S electrode reveals superior sulfur utilization ability based on the advantageous constitute and architecture, as illustrated in Fig. 4f. The porous framework provides effective ion penetration pathways and enough space for remission of volume expansion. Furthermore, the continuous carbon network with nitrogen doping can facilitate rapid electron transference and immobilize polysulfide through $LiS_xLi^+ \cdots N$ binding arising from the lone-pair electrons in nitrogen [46,47]. Consequently, the porous carbon incorporated Ni foam framework build an interconnected 3D conductive network to load sulfur, which improves the capacity and cycling performance of Li-S batteries.

In summary, we successfully designed and constructed a 3D freestanding conductive framework with nickel foam matrix and nitrogen doped porous carbon network for Li-S battery. The rationally designed Ni/PC-S freestanding electrode possesses a mutually embedded architecture with high stability. In the unique architecture, porous carbon incorporated nickel foam framework builds an interconnected 3D conductive network, which improves the low electrical conductivity of sulfur electrode and buffers volume variations sulfur during cycling. In addition, nitrogen doped carbon network relieves the diffusion of polysulfides and promotes the utilization of active sulfur. Consequently, the Ni/PC-S electrode delivers a high initial discharge capacity of around 1200 mAh/g and excellent cycling stability with slow capacity fading rate of 0.059% per cycle at 0.2 C after 500 cycles. In addition, a high rate capability (about 600 mAh/g at 2 C) is achieved. Importantly, even sulfur loading up to 4.2 mg/cm^2, high capacity retention of 84.2% can be retained at 1 C after 100 cycles. This work paves a simple way for design of freestanding porous electrodes with great potential application in energy storage and conversion devices.

Declaration of competing interest

The authors report no declarations of interest.

Acknowledgments

This study is financially supported by the National Natural Science Foundation of China (No. 21603109), the Henan Joint Fund of theNational Natural Science Foundation of China (No. U1404216).

Appendix A. Supplementary data

Supplementary material related to this article can be found, in the online version, at doi:https://doi.org/10.1016/j.cclet.2020.08.024.

References

[1] P.G. Bruce, S.A. Freunberger, L.J. Hardwick, J.M. Tarascon, Nat. Mater. 11 (2012) 19–29.
[2] Y.X. Yin, S. Xin, Y.G. Guo, L.J. Wan, Angew. Chem. Int. Ed. 52 (2013) 13186–13200.
[3] F. Li, Q. Liu, J. Hu, et al., Nanoscale 11 (2019) 15418–15439.
[4] H.J. Peng, J.Q. Huang, X.B. Cheng, Q. Zhang, Adv. Energy Mater. 7 (2017) 1700260.
[5] D. Liu, C. Zhang, G. Zhou, et al., Adv. Sci. 5 (2018) 1700270.
[6] Z. Ye, Y. Jiang, L. Li, F. Wu, R. Chen, Adv. Mater. 32 (2020) 2002168.
[7] J. Sun, J. Liang, J. Liu, et al., Energy Environ. Sci. 11 (2018) 2509–2520.
[8] J. He, A. Manthiram, Adv. Energy Mater. 10 (2020) 1903241.
[9] J. Wang, Y. Cui, D. Wang, Adv. Mater. 31 (2019) 1801993.
[10] J. Park, S.H. Yu, Y.E. Sung, Nano Today 18 (2018) 35–64.
[11] Y. Boyjoo, H. Shi, E. Olsson, et al., Adv. Energy Mater. 10 (2020) 2000651.
[12] R. Wang, J. Yang, X. Chen, et al., Adv. Energy Mater. 10 (2020) 1903550.
[13] Y. Song, H. Wang, Q. Ma, et al., New J. Chem. 43 (2019) 9641–9651.
[14] W. Ma, Q. Xu, Rare Met. 37 (2018) 929–935.
[15] Y. Liu, C. Song, Y. Wang, et al., Chem. Eng. J. 401 (2020) 126038.
[16] Q. Wang, K. Ye, L. Xu, et al., Chem. Commun. 55 (2019) 14801–14804.
[17] A. Fu, C. Wang, F. Pei, et al., Small 15 (2019) 1804786.
[18] F. Pei, A. Fu, W. Ye, et al., ACS Nano 13 (2019) 8337–8346.
[19] X. Qin, J. Wu, Z.L. Xu, et al., Carbon 141 (2019) 16–24.
[20] Y. Song, H. Wang, Q. Ma, et al., ACS Sustain. Chem. Eng. 7 (2019) 3042–3051.
[21] Z. Song, X. Lu, Q. Hu, et al., J. Power Sources 421 (2019) 23–31.
[22] D. Cai, B. Liu, D. Zhu, et al., Adv. Energy Mater. 10 (2020) 1904273.
[23] Z. Du, X. Chen, W. Hu, et al., J. Am. Chem. Soc. 141 (2019) 3977–3985.
[24] S. Jiang, S. Huang, M. Yao, et al., Chin. Chem. Lett. 31 (2020) 2347–2352.
[25] C. He, R. Wang, H. Yang, S. Li, L. Fu, Appl. Surf. Sci. 507 (2020) 145076.
[26] N. Song, Z. Gao, Y. Zhang, X. Li, Nano Energy 58 (2019) 30–39.
[27] B. Xu, S. Qi, M. Jin, et al., Chin. Chem. Lett. 30 (2019) 2053–2064.
[28] Z. Wei, B. Ding, H. Dou, et al., Chin. Chem. Lett. 30 (2019) 2110–2122.
[29] D. Zhou, C. Li, F. Yin, X. Tang, C. Pu, Chin. Chem. Lett. 31 (2020) 2325–2329.
[30] S. Zhao, R. Fang, Z. Sun, et al., Small Methods 2 (2018) 1800067.
[31] W. Cai, G. Li, D. Luo, et al., Adv. Energy Mater. 8 (2018) 1802561.
[32] S. Lin, Y. Yan, Z. Cai, L. Liu, X. Hu, Small 14 (2018) 1800616.
[33] Y. Chen, S. Niu, W. Lv, C. Zhang, Q. Yang, Chin. Chem. Lett. 30 (2019) 521–524.
[34] X. Yu, J. Deng, R. Lv, et al., Energy Storage Mater. 20 (2019) 14–23.
[35] S.S. Chi, Y. Liu, W.L. Song, L.Z. Fan, Q. Zhang, Adv. Funct. Mater. 27 (2017) 1700348.
[36] L. Liu, Y.X. Yin, J.Y. Li, et al., Adv. Mater. 30 (2018) 1706216.
[37] Ş. Sörgel, O. Kesten, A. Wengel, T. Sörgel, Energy Storage Mater. 10 (2018) 223–232.
[38] R. Li, Z. Bai, W. Hou, et al., Chin. Chem. Lett. 31 (2020), doi:http://dx.doi.org/10.1016/j.cclet.2020.03.048.
[39] H. Tang, J. Yang, G. Zhang, et al., Nanoscale 10 (2018) 386–395.
[40] H. Ye, D. Lei, L. Shen, et al., Chin. Chem. Lett. 31 (2020) 570–574.
[41] J. Yu, J. Xiao, A. Li, et al., Angew. Chem. Int. Ed. 59 (2016) 3374–3382.
[42] R. Fang, S. Zhao, P. Hou, et al., Adv. Mater. 28 (2016) 3374–3382.
[43] Y.T. Liu, S. Liu, G.R. Li, T.Y. Yan, X.P. Gao, Adv. Sci. 7 (2020) 1903693.
[44] V. Knap, D.I. Stroe, M. Swierczynski, R. Teodorescu, E. Schaltz, J. Electrochem. Soc. 163 (2016) A911–A916.
[45] S.H. Chung, A. Manthiram, ACS Energy Lett. 2 (2017) 1056–1061.
[46] X. Tao, J. Wang, C. Liu, et al., Nat. Commun. 7 (2016) 11203.
[47] M. Xiang, H. Wu, H. Liu, et al., Adv. Funct. Mater. 27 (2017) 1702573.